

Few-layer Binder Free Graphene Modified Mercury Film Electrode for Trace Metal Analysis by Square Wave Anodic Stripping Voltammetry

Salma Zbeda, Keagan Pokpas, Salam Titinchi, Nazeem Jahed*, Priscilla G. Baker and Emmanuel I. Iwuoha

SensorLab, Department of Chemistry, University of the Western Cape, Bellville 7535, South Africa;

*E-mail: njahed@uwc.ac.za

Received: 14 June 2013 / Accepted: 9 July 2013 / Published: 20 August 2013

A binding agent free graphene modified glassy carbon electrode in combination with an *in situ* plated mercury film electrode (Gr-GC-HgFE) was used as a highly sensitive electrochemical platform for the determination of Zn^{2+} , Cd^{2+} and Pb^{2+} in 0.1 M acetate buffer (pH 4.6) by square-wave anodic stripping voltammetry (SWASV). Instrumental parameters such as deposition potential, deposition time and electrode rotation speed were optimized. The Gr-GC-HgFE sensing platform exhibited improved sensitivity for metal ion detection, in addition to well defined, reproducible and sharp stripping signals. Two linear calibration curves ranging from 0 – 10 $\mu g L^{-1}$ and 0 – 60 $\mu g L^{-1}$ were identified yielding detection limits of 0.08 $\mu g L^{-1}$, 0.05 $\mu g L^{-1}$ and 0.14 $\mu g L^{-1}$ for Zn^{2+} , Cd^{2+} and Pb^{2+} , respectively, for simultaneous analysis and 0.04 $\mu g L^{-1}$, 0.11 $\mu g L^{-1}$ and 0.14 $\mu g L^{-1}$ for Zn^{2+} , Cd^{2+} and Pb^{2+} , respectively, for individual analysis when using a deposition time of 120 s. For practical applications recovery studies using tap water samples spiked with target metal ions gave recoveries within 10% of the spiked amount. Much better recoveries were obtained for the individual analysis in comparison with simultaneous analysis.

Keywords: Graphene, modified mercury film, square wave anodic stripping voltammetry, heavy metals

1. INTRODUCTION

Heavy metals pollution of the environment is a mounting problem worldwide and is a cause for concern [1-3] owing to its deleterious health effects [4,5]. As a consequence, a variety of techniques are being used to detect trace amounts of heavy metals, including atomic absorption spectrometry (AAS), inductively coupled plasma optical emission spectrometry (ICP-OES), X-ray fluorescence (XRF) and electrochemical stripping techniques such as, anodic stripping voltammetry (ASV) [6].

Electrochemical stripping techniques are economical, portable and have easy process procedures [6] in addition the anodic stripping voltammetric technique is capable of measuring four to six analytes in a sample simultaneously in the sub-parts per billion (sub-ppb) range [7,8].

Mercury thin film electrodes (HgFEs) are widely used for anodic stripping voltammetric (ASV) determination of mercury soluble trace elements [9]. The film is deposited on an inert substrate, typically, a glassy carbon electrode (GCE). HgFEs may be prepared in a pure mercury(II) solution (*ex situ*), after which the electrode is transferred into the sample solution or, they may be formed *in situ* by simply adding mercury(II) ions into the medium to be analyzed. The rate of mercury deposition is a function of the pH of the electrolyte, deposition potential, stirring rate and mercury ion concentration. Optical examinations of the mercury film electrodes revealed the formation of fewer and larger drops instead of a homogeneous film [10].

Graphene, a two-dimensional (2D) honey-comb lattice of carbon atoms [11] has recently appeared as an exciting material for electronics due to fast electron transporter movement in bulk graphene [12], low density and large specific surface area [13].

Recently graphene has been used improve the sensitivity of metal detection due to its unusual electronic, thermal and mechanical properties [14-19]. Wang's group [20,21] have confirmed the usefulness of the graphene nano-sheets in developing a high-sensitivity sensor for the determination of lead and cadmium ions. Khomyakov *et al.* [22] evidenced the interaction and charge transfer between graphene and metal ions and concluded that the interaction and the charge transfer between graphene and metal ions made the modified electrode much more sensitive. Previous researchers have shown that graphene mixed with a binding agent such as nafion and then drop coated onto a GCEs surface have successfully been used to detect trace heavy metals ions in water samples [21,23]. Furthermore, Wong *et al.* has recently showed that a glassy carbon electrode (GCE) modified with chemically reduced graphene oxide and without using any binding agent can be used for the determination of cadmium [24].

In this work graphene was prepared by the chemical reduction of graphene oxide and used to modify the GCE without the use of binding agents followed by the *in situ* deposition of a Hg film (Gr-GC-HgFE). The new electrode (Gr-GC-HgFE) was investigated for its applicability towards the determination of Zn^{2+} , Cd^{2+} and Pb^{2+} ions in water.

2. EXPERIMENTAL SECTION

2.1. Reagents

All chemicals used in this study were analytical reagent grade and used without further purification. Standard stock solutions ($1,000\text{ mg L}^{-1}$, atomic absorption standard solution) were obtained from Sigma-Aldrich and diluted as required.

The 0.1 M acetate buffer (pH 4.6) was used as supporting electrolyte and prepared by mixing glacial acetic acid and sodium acetate followed by diluting the solution with ultra pure distilled water (Millipore). A pH meter (Metrohm 827 pH lab.) was calibrated using pH 4 and pH 7 calibration buffer

solutions and, then used to verify the pH of the acetate buffer (supporting electrolyte) solution.

2.2. Apparatus

Square-wave anodic stripping voltammetry (SWASV) measurements were carried out using a 797 VA COMPUTRACE instrument connected to a personal computer. The graphene modified glassy carbon mercury film electrode (Gr-GC-HgFE) served as the working electrode. An Ag/AgCl (saturated KCl) and platinum wire served as the reference and counter electrodes, respectively. All electrochemical measurements were carried out in a 20 mL cell.

Fourier Transform Infrared (FT-IR) spectra were recorded using a (Perkin Elmer Spectrum 100) coupled to an Attenuated Total Reflectance (ATR) sample holder. FT-IR was used to obtain information and confirmation on graphene or graphene oxide. Scanning Electron Microscopy (SEM) measurements were performed using a LEO 1450 SEM 30 kV instrument equipped with Electronic Data System (EDS) and Windows Deployment Services (WDS); images were taken using the secondary electron detector. The samples were dried in a vacuum oven and deposited on the silicon grid surface before SEM observations. High Resolution Transmission Electron Microscopy (HRTEM) measurements were carried out with a Tecnai G2 F20X-Twin MAT Field Emission Transmission Electron Microscope from FEI (Eindhoven, Netherlands) under an acceleration voltage of 200 kV. The samples were prepared by dropping a dilute suspension of graphene or graphene oxide in ethanol onto copper grids followed by air drying at room temperature. XRD measurements were carried out using a Bruker AXS D8 Advance diffractometer from BRUKER- AXS Germany with Cu-K α radiation and Raman spectroscopy was obtained using a Dilor XY Raman spectrometer with a Coherent Innova 300 Argon laser with a 514.5 nm laser excitation.

2.3. Synthesis of graphene (Gr)

Graphene used in this experiment was prepared by chemically reducing graphene oxide. Graphene oxide (GO) was synthesized from natural graphite using the modified Hummers method [25]. 50 mg of GO was added to 50 ml of distilled water and sonicated for 1 hour. A 0.15 g of sodium borohydride (NaBH₄) was added and the mixture stirred for 30 minutes. The mixture was then heated at 125 °C under reflux for 3 hours. The resulting black precipitate was centrifuged, washed with water, ethanol and dried in vacuum oven. [26].

2.4. Preparation of Modified Electrode (Gr -GCE)

A glassy carbon electrode was polished with alumina powder in the order 1, 0.3 and 0.05 micron respectively, on a wet polishing cloth by pressing the electrode softly against the polishing surface. The electrode rinsed with ultra pure distilled water and polished again with ethanol on a clean polishing cloth. The electrode was then cycled (10 times) between -1.3 and -0.2 V in 6 M nitric acid to remove any other impurities. A SWASV run was then done in 0.1 M acetate buffer to check for any

spurious peaks prior to modifying the glassy carbon electrode. A 0.25 mg mL^{-1} of graphene solution in ethanol was sonicated for 30 minutes or until fully dispersed. Afterwards, $1 \mu\text{L}$ of the graphene suspension was drop coated onto the glassy carbon electrode (GCE) and allowed to dry at room temperature to give the graphene modified glassy carbon electrode (Gr-GCE).

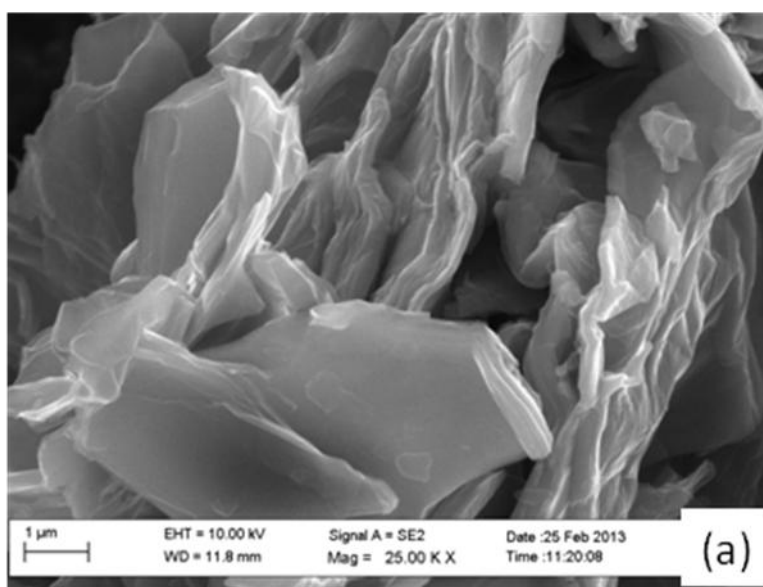
2.5. Procedure for SWASV Analysis

Firstly, the cell, Teflon stirrer, counter electrode and reference electrode were cleaned with 6 M nitric acid and rinsed with distilled water. 20 ml of 0.1 M acetate buffer solution (pH 4.6) was pipeted into the voltammetric cell. Subsequently, Hg^{2+} and target metal ions were added to the solution and stirred for 10 s. The stirring was stopped and the solution allowed to equilibrate for 10 s. The voltammogram was then recorded by applying a potential from -1.4 V to 0.6 V using SWASV with rotation speed 1000 rpm, voltage step 0.005951 V and frequency 50 Hz. A cleaning step of 60 s at 0.3 V, with the solution stirring was used to remove the target metals and metal film.

3. RESULTS AND DISCUSSION

3.1. Scanning Electron Microscopy (SEM)

The SEM images of GO and graphene are shown in Figure 1. A SEM image of feathery GO powder Figure 1(a), shows an agglomeration of the exfoliated platelets. It is noticed that the GO shows an uneven surface probably owing to the oxidation of sheets [27]. The SEM image of graphene in Figure 1(b) reveals that the material consists of thin, haphazardly aggregated, wrinkly sheets closely linked with each other forming a lawless solid [28].



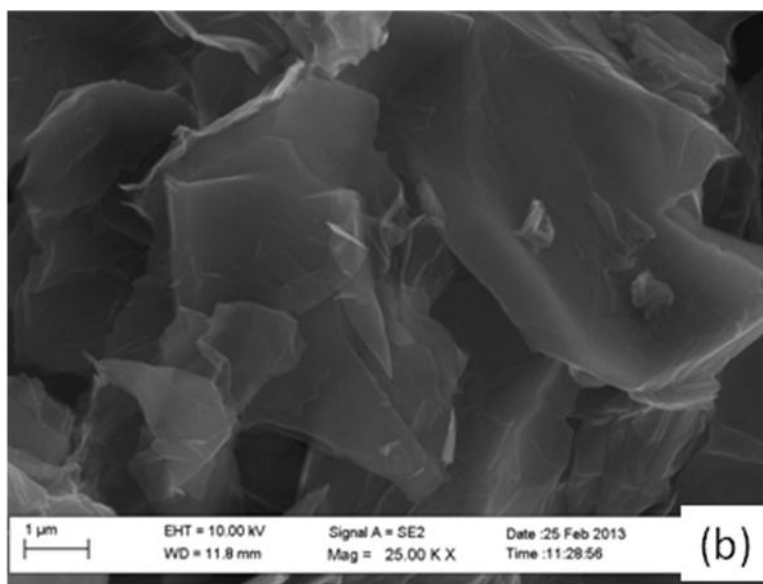


Figure 1. SEM images for (a) graphene oxide and (b) graphene

3.2. High Resolution Transmission Electron Microscopy (HRTEM)

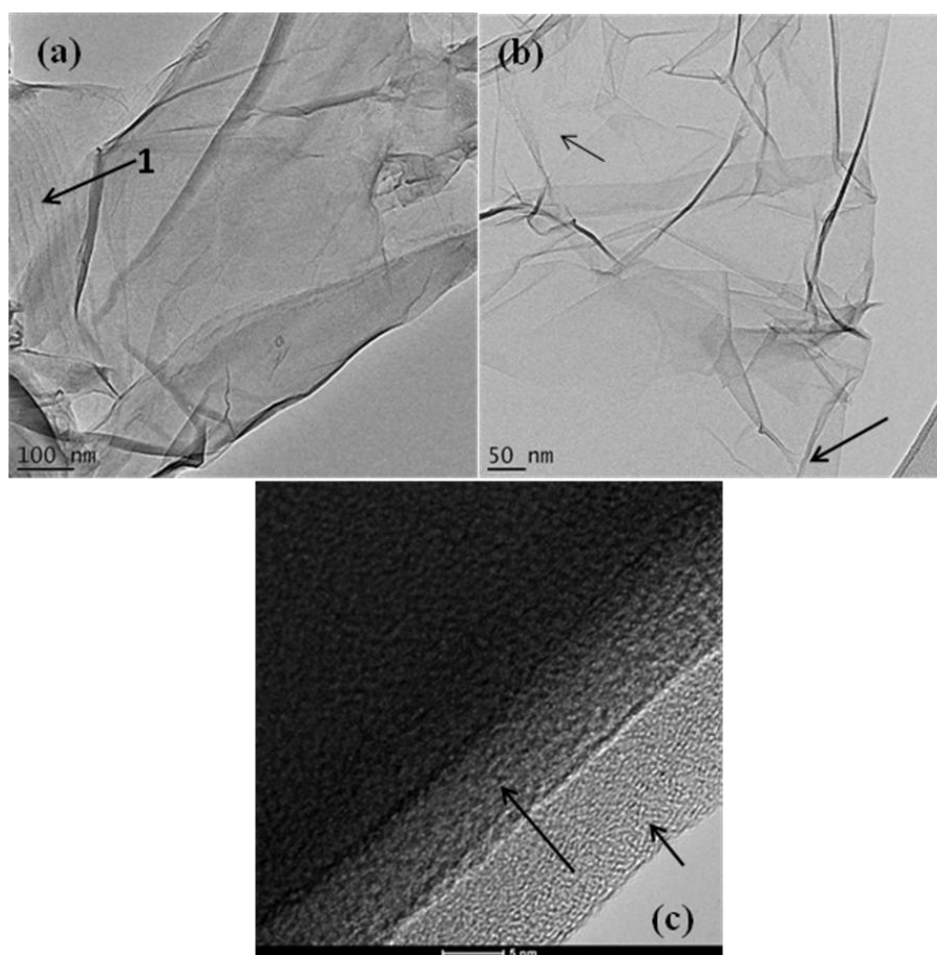


Figure 2. TEM images of (a) graphene oxide, (b) graphene and (c) graphene layers

The HRTEM images of GO and graphene are shown in Figure 2. The GO image [Figure 2(a)], shows that the sample is a layered structure (indicated by arrow 1) consisting of stacked GO sheets in addition, the larger transparent sheets resemble wavy silk veils entangled with each another [27]. The HRTEM image for graphene Figure 2(b), shows a crumpled and wrinkled transparent flake-like structure. The most transparent and featureless regions suggest (indicated by arrows) monolayer graphene [29]. At higher magnification the HRTEM image [Figure 2(c)] show the monolayers of graphene.

3.3. Fourier Transformed Infrared Spectroscopy (FT-IR)

Previous researches have shown that the surfaces of graphene oxide are covered with a variety of oxygen functional groups namely, hydroxyl, ethers, epoxides, carbonyl and carboxylic groups [30,31]. The FT-IR spectra of GO and graphene are shown in Figure 3. Graphene oxide showed a large compilation of diffused bands. The peak at 1406 cm^{-1} is due to C–OH stretching vibrations, whereas, the band at 1602 cm^{-1} is attributed to the aromatic C=O group. A peak at 1023 cm^{-1} is associated with C–O vibrations from alkoxy groups [32], while the deformation of the C–O was observed at 1159 cm^{-1} . The peak at 1279 cm^{-1} is associated with the bending of the O–H group [33]. The peak at 2666 cm^{-1} corresponds to an asymmetric C–H stretching vibration [34]. After reduction with NaBH_4 greater part of the above mentioned bands are notably reduced or completely removed demonstrating that all or most of the oxygen was removed.

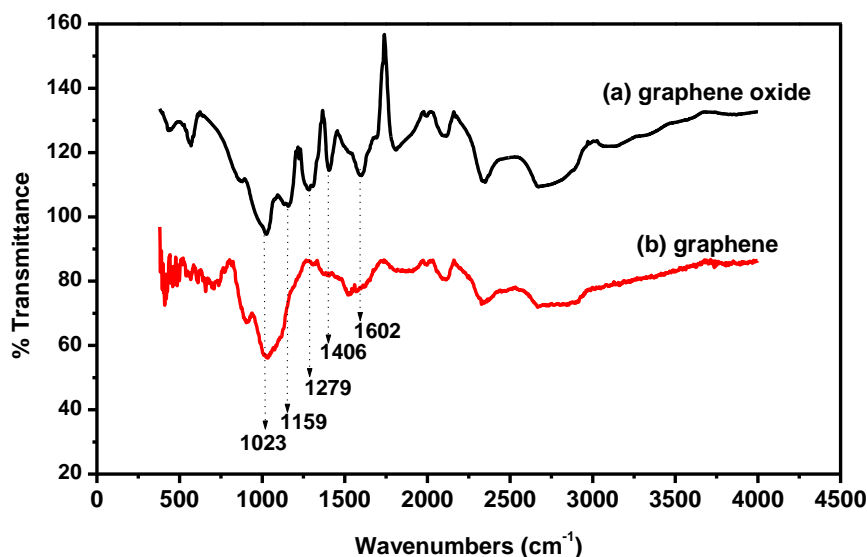


Figure 3. FT-IR spectra of (a) graphene oxide and (b) graphene

3.4. X-ray Diffraction (XRD)

The XRD analysis of GO and graphene are shown in Figure 4. GO shows a sharp, tall peak at 10° corresponding to the presence of oxygen containing functional groups formed during oxidation;

these functional groups cause the GO sheets to stack more loosely [35]. The broad peak at 25° may be due to appearance of exfoliated sheets, while the peak at 42.5° corresponds to the 100 crystal plane. After reduction of graphene oxide to graphene the peak at 9.1° disappeared and a broad peak centred at 25° is observed. The broadness of this 25° peak could be due to increased disorder in the through-plane direction of the graphene sample and, also perhaps due to structural defects from sonication [36].

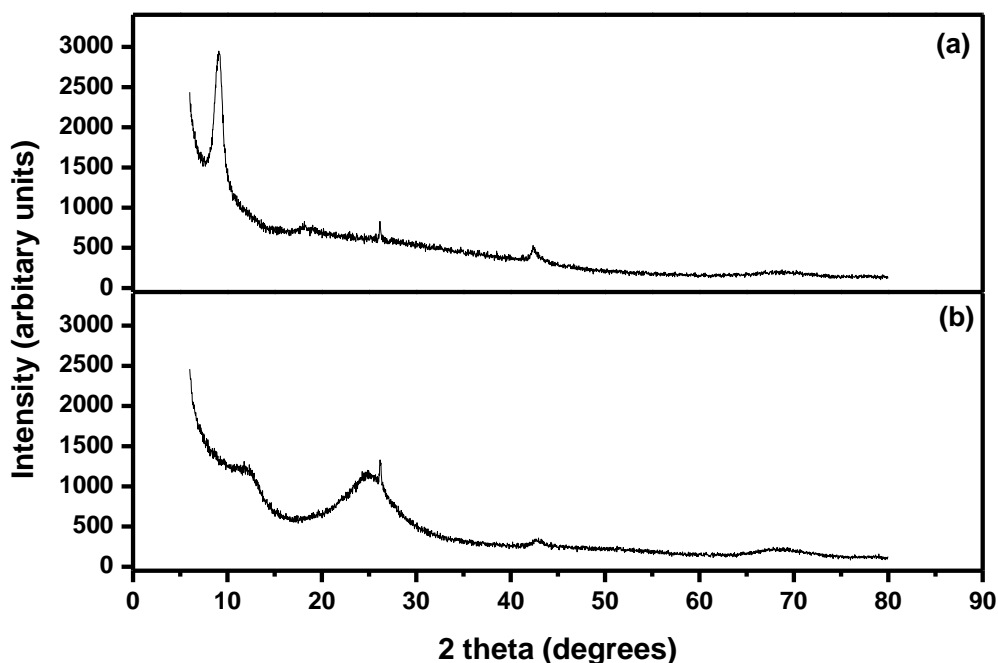


Figure 4. XRD diffractograms for (a) graphene oxide and (b) graphene.

3.5. Raman Spectroscopy

The Raman spectra of graphene and graphene oxide are shown in Figure 4.5. The Raman spectrum of graphene includes the D peak located at 1348 cm^{-1} , G peak at 1591 cm^{-1} and 2D peak at 2866 cm^{-1} . The D peak is due to the presence of confusion in atomic arrangement or edge effect of graphene whilst, the G peak due to in-plane vibration of the sp^2 carbon atoms. The 2D band appears at almost double the frequency of the D band and originates from second order Raman scattering process [37,38]. For GO, the G band is broadened and shifted to 1604 cm^{-1} , and the D peak at 1345 cm^{-1} is absent. The ratio of the intensities (I_D/I_G) for GO is 0.98 while it increased for graphene to 1.08. This increase is attributed to the significant decrease in size of the in-plane sp^2 domains due to oxidation and ultrasonic exfoliation, and somewhat disordered graphite crystal structure of graphene nanoplatelets [39].

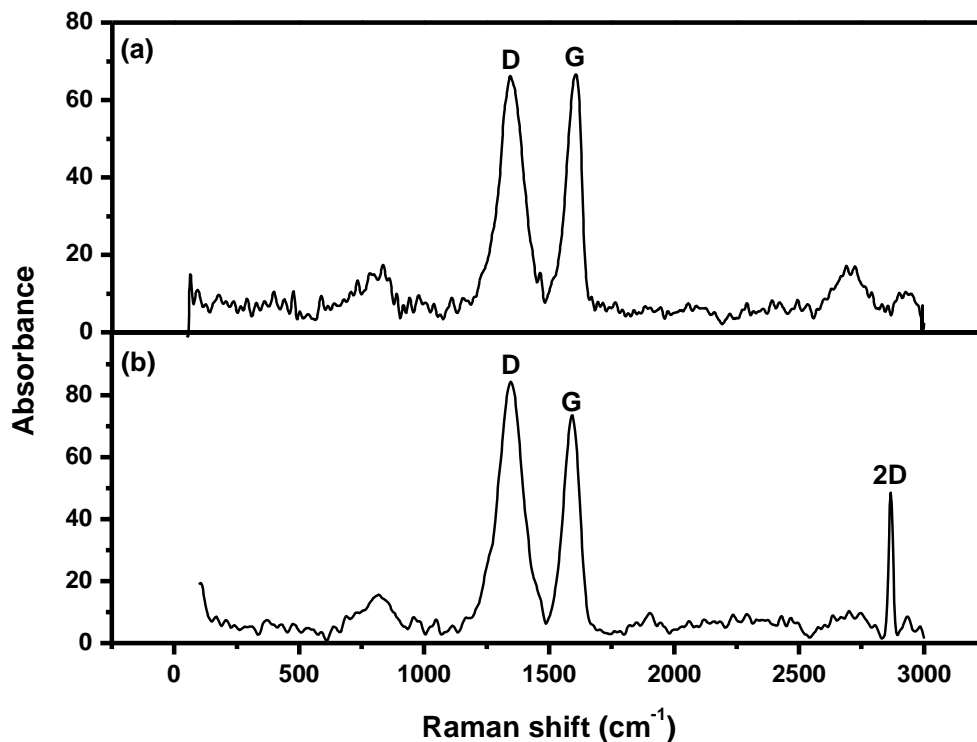


Figure 5. Raman spectra of (a) graphene oxide and (b) graphene.

3.6. Current responses at the graphene modified glassy carbon thin film mercury electrodes (Gr-GC-HgFE)

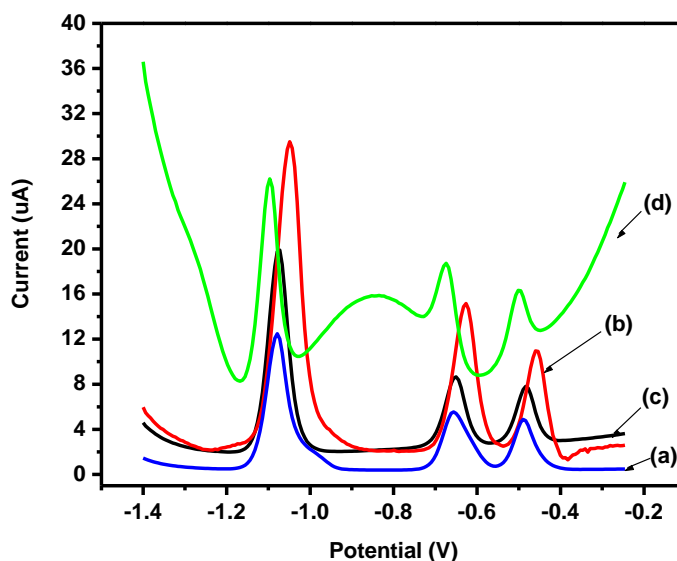


Figure 6. SWASV of 20 $\mu\text{g L}^{-1}$ of Zn^{2+} , Cd^{2+} and Pb^{2+} at a glassy carbon electrode (GCE) modified with (a) 0 mg ml^{-1} , (b) 0.25 mg ml^{-1} , (c) 0.5 mg ml^{-1} and (d) 1.0 mg ml^{-1} solutions of graphene with an *in situ* deposited Hg film. Supporting electrolyte (0.1 M acetate buffer pH 4.6), deposition time (120 s at -1.3 V), rotation speed (1000 rpm), frequency (50 Hz), amplitude (0.04 V) and sweep rate (0.2975 V s^{-1}).

Figure 6 shows the stripping voltammetric responses (peak currents) for $20 \mu\text{g L}^{-1}$ of each target metal ion (Zn^{2+} , Cd^{2+} and Pb^{2+}) in 20 ml of 0.1 M acetate buffer solution (pH 4.6) and 5 mg L^{-1} Hg^{2+} ions at the Gr-GC-HgFE. The stripping voltammetric peaks appear at approximately -1.1 V , -0.7 V and -0.5 V for Zn^{2+} , Cd^{2+} and Pb^{2+} , respectively. The peak currents show a gradual decrease when increasing concentrations of graphene solutions were used on to prepare the Gr-GC-HgFE; the highest peak currents being observed with 0.25 mg mL^{-1} of graphene solution. A plausible reason for this decrease in peak currents can be attributed to the increase in the number of graphene sheets stacking on top of each other as shown in, Figure 2(c) to form multilayers (at higher graphene concentrations). This stacking phenomenon hinders the passage of electron flow from the analyte solution to the GCE surface.

The absence of an *in situ* deposited Hg-film on the graphene modified GC electrode (Gr-GCE) is also noticeable in Figure 7. The stripping voltammograms recorded at the Gr-GC-HgFE shows an increase in peak currents for all three metal ions whereas, no peak current for Zn^{2+} is observed at the Gr-GCE. The non-response for Zn^{2+} indicates that zinc is not sufficiently deposited onto the Gr-GCE hence, no stripping zinc peak is observed. It is evident from this result that enhanced sensitivity is achieved due to amalgam formation in the presence of an *in situ* deposited Hg-film. In general, the voltammetric peaks at the Gr-GC-HgFE show taller, symmetrical peaks for Cd^{2+} and Pb^{2+} in addition to a Zn^{2+} peak.

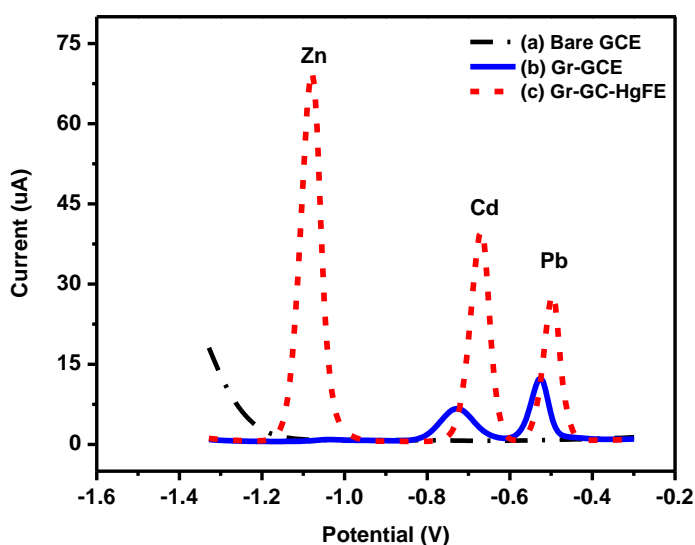


Figure 7. The effect of a mercury film on the peak current of $20 \mu\text{g L}^{-1}$ of Zn^{2+} , Cd^{2+} and Pb^{2+} at the Gr-GC-HgFE. Supporting electrolyte (0.1 M acetate buffer pH 4.6), deposition time (120 s at -1.3 V), rotation speed (1000), frequency (50 Hz), amplitude (0.04 V) and sweep rate (0.2975 V s^{-1}).

3.7. The Effect of Experimental Variables

The influence of deposition potential on the peak currents of Zn^{2+} , Cd^{2+} and Pb^{2+} at the Gr-GC-HgFE was studied in the potential range -0.4 V to -1.4 V . The voltammograms in Figure 8(a) show that

at potentials greater than their oxidation potentials of the target metal ions no response signals were observed since, no reduction of the metal ions from the analyte solution occurs. In general, the peak currents for all three metals increase as the deposition potential becomes more negative and is due to all three metals being positively charged ions, which are preferentially reduced at more negative potentials [40]. Thus, to effect simultaneous deposition of the target metal ions (Zn^{2+} , Cd^{2+} and Pb^{2+}) a potential of -1.3 V was selected for further analysis.

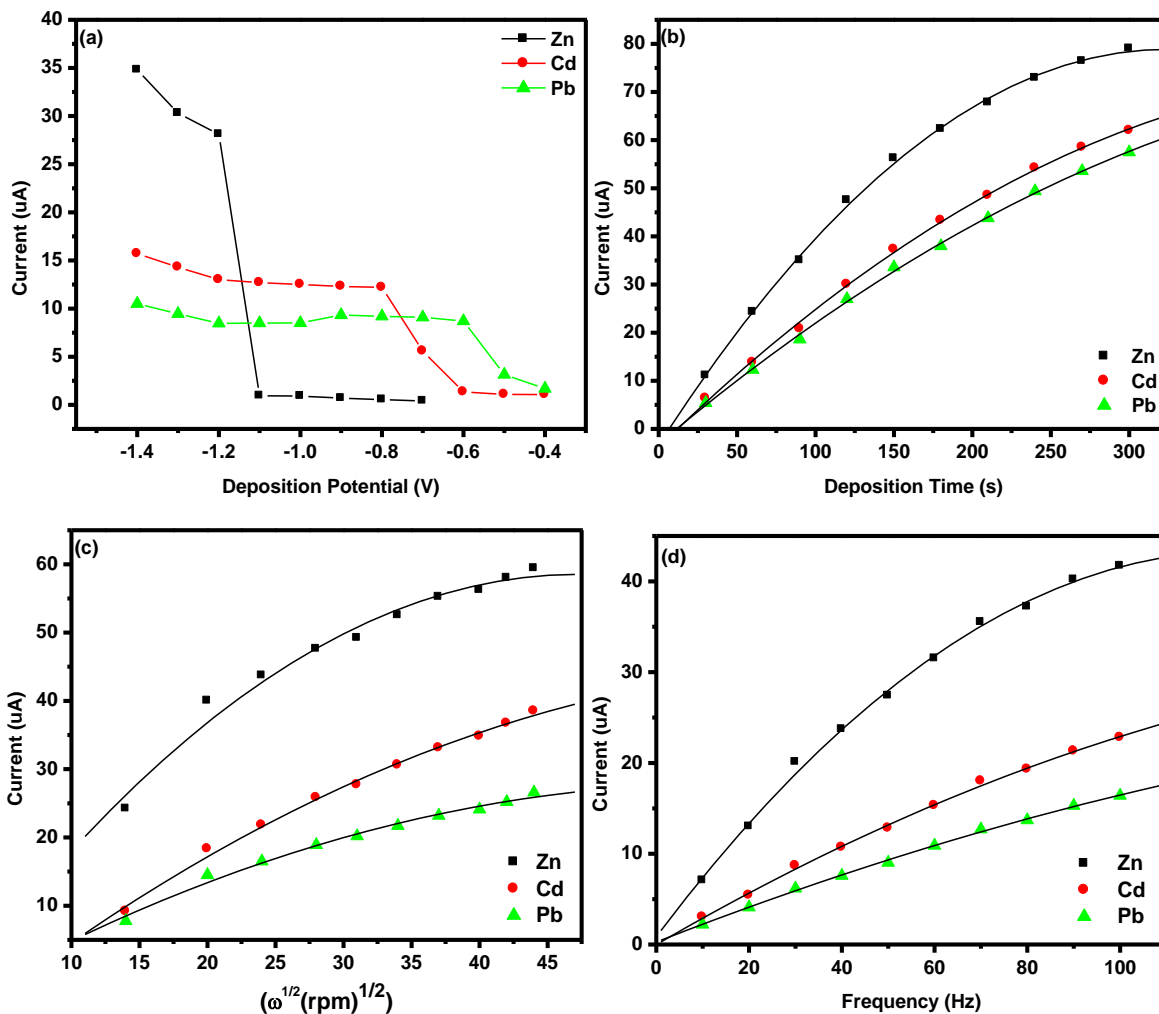


Figure 8. The effect of (a) deposition potential, (b) deposition time, (c) rotation speed and (d) frequency and on the peak currents on $20 \mu\text{g L}^{-1}$ of Zn^{2+} , Cd^{2+} and Pb^{2+} at the Gr-GC-HgFE in supporting electrolyte (0.1 M acetate buffer pH 4.6).

Figure 8(b) shows that the peak currents of the metals ions increase rapidly with increasing deposition time from 30 to 200 s since more time is allowed for the analyte ions to undergo reduction and deposition at the Gr-GC-HgFE surface. At deposition times greater than 200 s there is a gradual decrease in response due to surface saturation of the electrode [40]. A deposition time of 120 s was chosen for subsequent experiments to avoid possible surface saturation beyond 120 s.

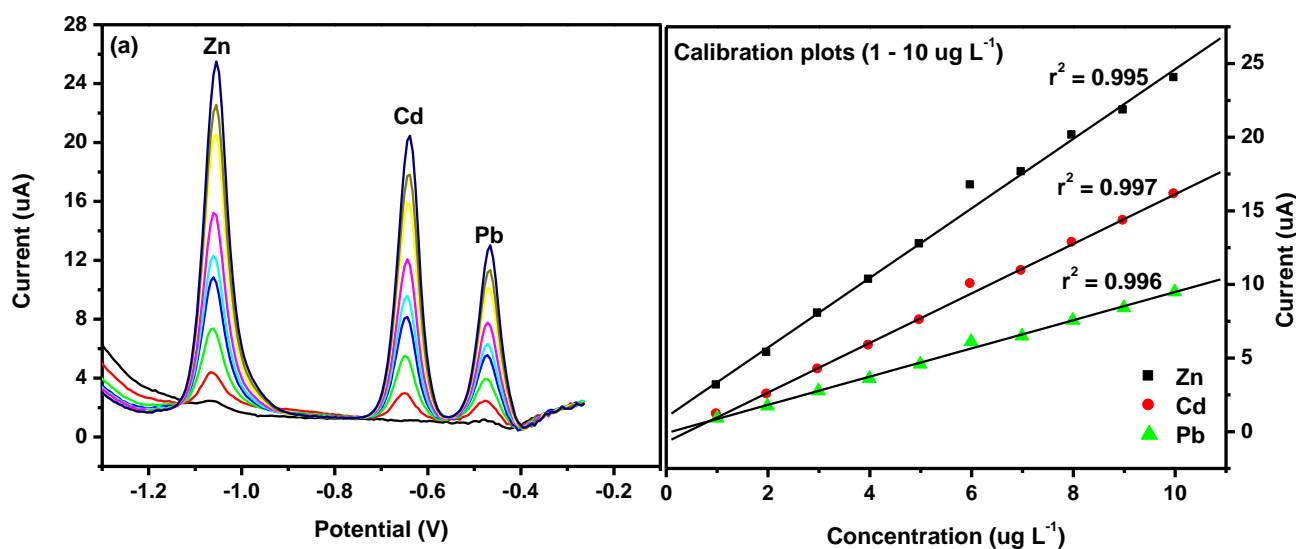
The effect of rotation speed on the peak currents of Zn^{2+} , Cd^{2+} and Pb^{2+} applied to the Gr-GC-HgFE was studied from 200 – 2000 rpm and is shown in Figure 8(c). As the square-root of rotation speed increases so does the stripping peak currents of metal ions. The rotation speed enhances the sensitivity of stripping analysis since it facilitates the migration of metal ions from the bulk analyte solution to the electrode surface where reduction of the ions takes place. A rotation speed of 1000 rpm was chosen for further experiments. Figure 8(d) shows the variation of frequency with the peak currents of Zn^{2+} , Cd^{2+} and Pb^{2+} applied over the frequency range from 10 to 100 Hz. As the frequency increased so did the peak current of all the metal ions, since the effective scan rate increases [41]. A frequency of 50 Hz was chosen as the optimum frequency.

3.8. Film stability and reproducibility

The peak currents of Zn^{2+} , Cd^{2+} and Pb^{2+} remained almost the same each time a new Gr-GC-HgFE was prepared and used to detect $20 \mu\text{g L}^{-1}$ of each metal ion in 20 ml of acetate buffer (pH 4.6), at the same conditions. The percentage relative standard deviation (RSD %) for the oxidation peaks was 1.13, 4.7 and 2 % for Zn^{2+} , Cd^{2+} and Pb^{2+} , respectively, this indicates the excellent reproducibility in preparing the Gr-GC-HgFE.

3.9. Analytical Performance at the graphene modified glassy carbon thin film mercury electrode (Gr-GC-HgFE)

The simultaneous and individual analysis of Zn^{2+} , Cd^{2+} and Pb^{2+} ions was conducted over two linear ranges namely, a low range ($1 - 10 \mu\text{g L}^{-1}$) and a high range ($5 - 60 \mu\text{g L}^{-1}$) at the Gr-GC-HgFE in order to determine the analytical performance of the electrode. During simultaneous analysis all three metal ions are present in the same solution and the peak currents obtained from the voltammograms was used to construct the calibration curves in Figures 9(a) and (b). Similarly, the calibration curves for the individual analysis Zn^{2+} , Cd^{2+} and Pb^{2+} ions over two linear ranges the low range ($1 - 10 \mu\text{g L}^{-1}$) presented in Figure 10 and a high range ($5 - 60 \mu\text{g L}^{-1}$) not presented here.



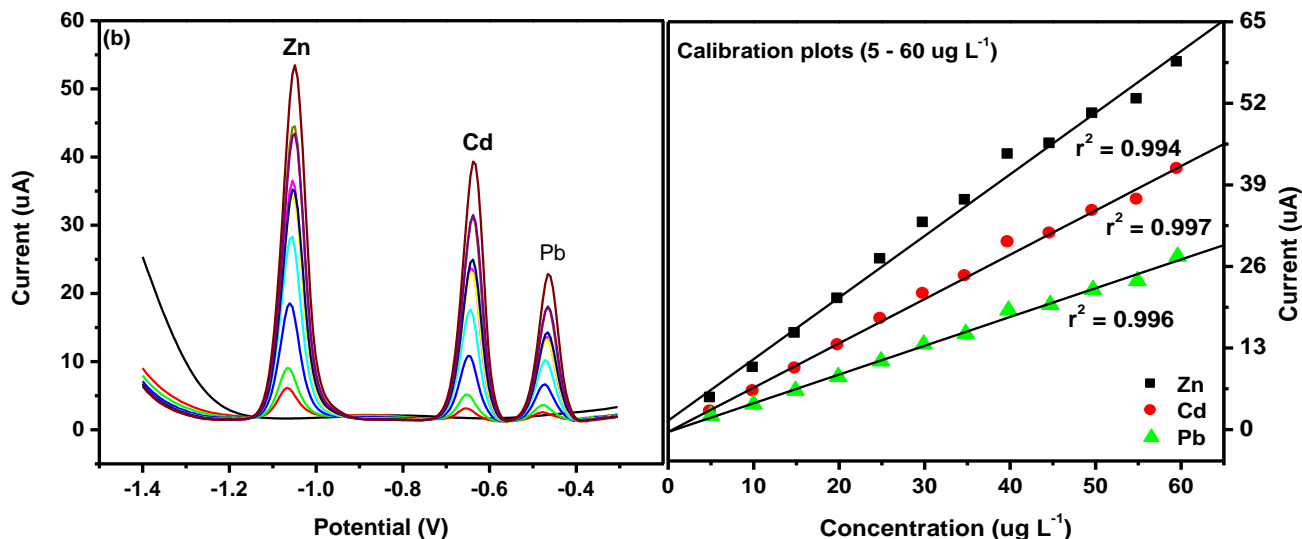
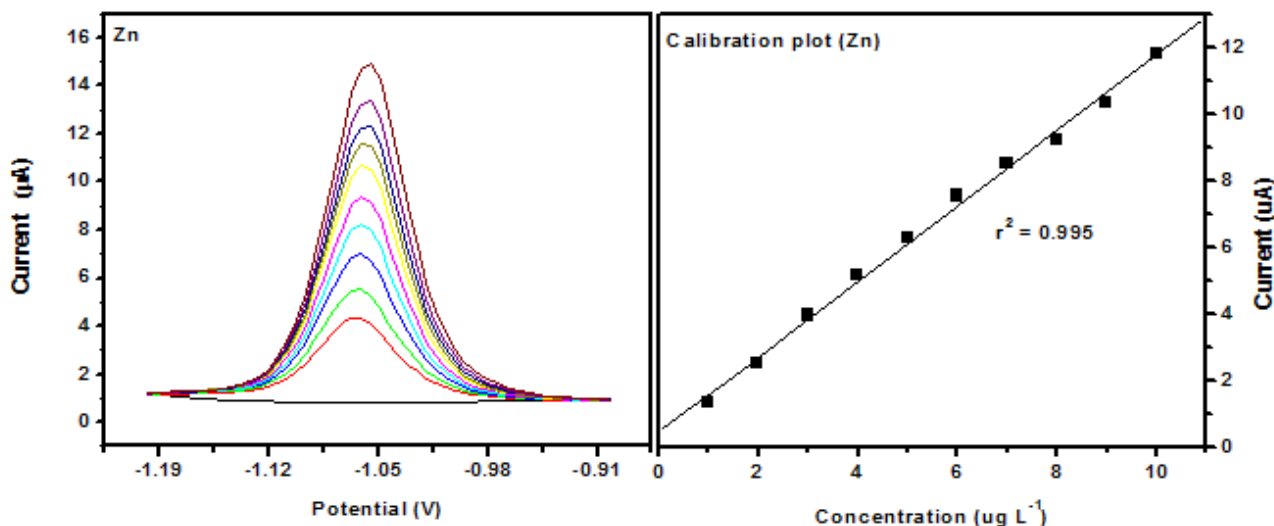


Figure 9. Square wave anodic stripping voltammograms and corresponding calibration plots of Zn²⁺, Cd²⁺ and Pb²⁺ obtained at the Gr-GC-HgFE over two concentration ranges (a) 1 – 10 μg L⁻¹ and (b) 5 - 60 μg L⁻¹. Supporting electrolyte (0.1 M acetate buffer pH 4.6), deposition time (120 s at -1.3 V), rotation speed (1000 rpm), frequency (50 Hz), amplitude (0.04 V) and sweep rate (0.2975 V s⁻¹).

From the calibration curves in Figures 9 and 10, the detection limits of the metal ions were determined based on three times the standard deviation ($3\sigma_{\text{blank}}$) of the blank divided by the slope of the calibration curve. The standard deviation of the blank was calculated from ten replications in the presence of Hg²⁺ ions. The detection limits and the correlation coefficients for the simultaneous and individual analysis of the metal ions are shown in the Tables 1 and 2, respectively.

In comparing, the detection limits ($3\sigma_{\text{blank}}/\text{slope}$) in Tables 1 and 2 the same deposition time (of 120 s) was used for both individual and simultaneous determinations. The detection limits for individual analysis were lower in comparison to those for simultaneous analysis.



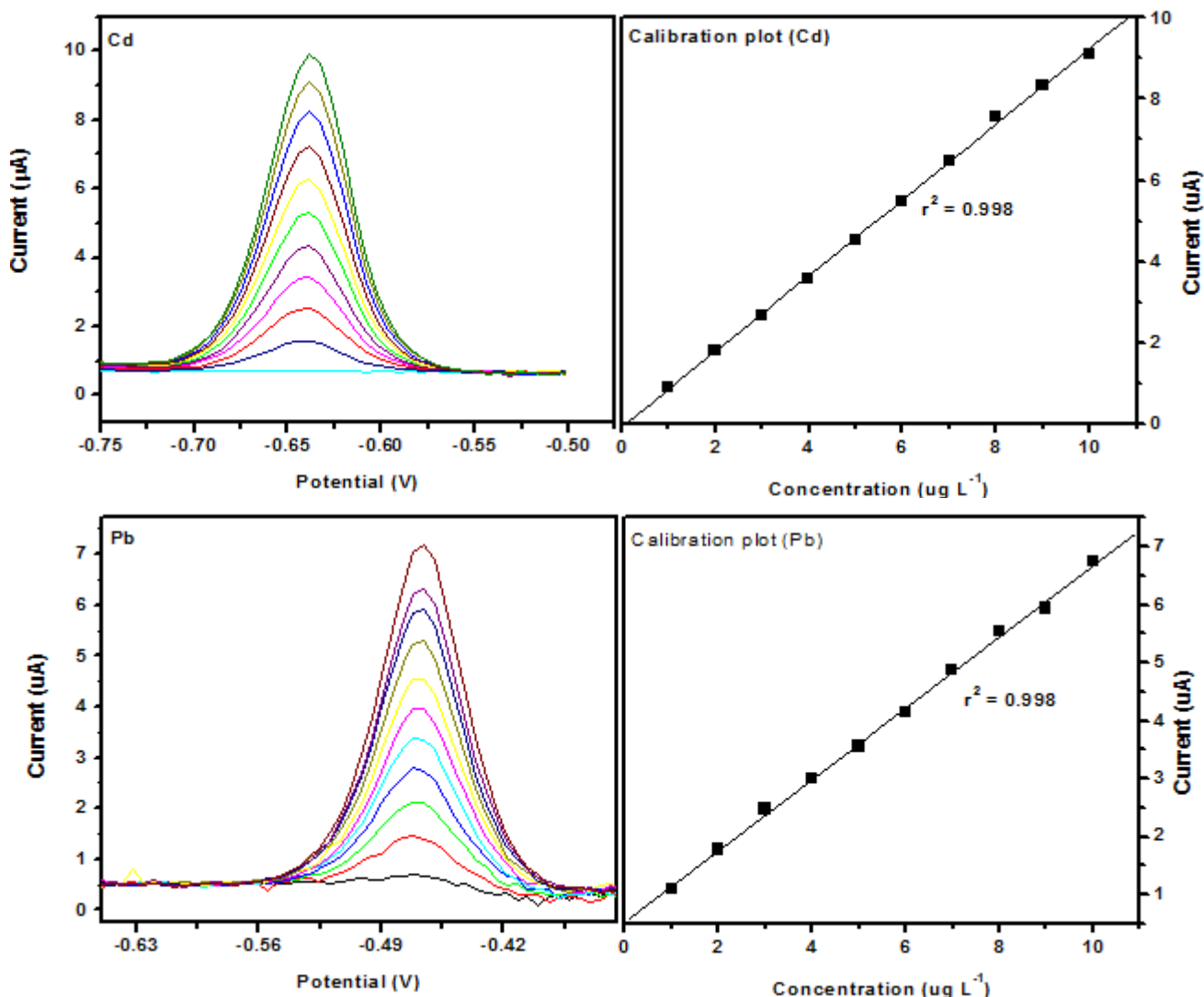


Figure 10. Square wave anodic stripping voltammograms and corresponding calibration plots of Zn^{2+} , Cd^{2+} and Pb^{2+} obtained at the Gr-GC-HgFE over the concentration range, $1 - 10 \mu g L^{-1}$. Supporting electrolyte (0.1 M acetate buffer pH 4.6), deposition time (120 s at -1.3 V), rotation speed (1000 rpm), frequency (50 Hz), amplitude (0.04 V) and sweep rate ($0.2975 V s^{-1}$).

Table 1. Correlation coefficients, (r^2), and detection limits for Zn^{2+} , Cd^{2+} and Pb^{2+} determined simultaneously at the Gr-GC-HgFE.

Analytical parameters	Range 1 - $10 \mu g L^{-1}$			Range 5 - $60 \mu g L^{-1}$		
	Zn^{2+}	Cd^{2+}	Pb^{2+}	Zn^{2+}	Cd^{2+}	Pb^{2+}
Slope ($\mu A L \mu g^{-1}$)	2.65	1.99	0.96	0.84	0.66	0.41
Standard deviation of blanks (μA)	0.070	0.035	0.046	0.050	0.038	0.057
Correlation coefficient (r^2)	0.995	0.997	0.996	0.994	0.997	0.996
Detection limit ($\mu g L^{-1}$)	0.08 (± 0.010)	0.05 (± 0.009)	0.14 (± 0.001)	0.18 (± 0.020)	0.17 (± 0.009)	0.42 (± 0.035)

*n = 3, where n is the number of replications.

Table 2. Correlation coefficients, (r^2) and the detection limits for Zn^{2+} , Cd^{2+} and Pb^{2+} determined individually at the Gr-GC-HgFE.

Analytical parameters	Range 1 -10 $\mu g L^{-1}$			Range 5 -60 $\mu g L^{-1}$		
	Zn^{2+}	Cd^{2+}	Pb^{2+}	Zn^{2+}	Cd^{2+}	Pb^{2+}
Slope ($\mu A L \mu g^{-1}$)	1.32	0.92	0.66	0.39	0.46	0.40
Standard deviation of blanks (μA)	0.018	0.035	0.030	0.019	0.018	0.036
Correlation coefficient (r^2)	0.995	0.998	0.998	0.993	0.994	0.994
Detection limits ($\mu g L^{-1}$)	0.04 (± 0.008)	0.11 (± 0.005)	0.14 (± 0.007)	0.15 (± 0.010)	0.12 (± 0.001)	0.27 (± 0.020)

*n = 3, where n is the number of replications

Table 2. Detection limits found from previous studies of Zn^{2+} , Cd^{2+} and Pb^{2+} at various electrodes.

Metal detected	Electrode substrate	Measurement technique	Deposition time (s)	Detection limit ($\mu g L^{-1}$)	Refs.
Cd^{2+} , Pb^{2+} , Zn^{2+}	Carbon based mercury thin film electrode	CV & (DPASV)	60	$Cd^{2+} = 0.25$ $Pb^{2+} = 0.08$ $Zn^{2+} = 5.5$	[43]
Pb^{2+} , Cd^{2+}	Thin-film Hg	SWASV	120	$Pb^{2+} = 1.8$ $Cd^{2+} = 2.9$	[44]
Pb^{2+} , Cd^{2+} , Zn^{2+}	Bi-C- nanotubes	SWASV	300	$Pb^{2+} = 1.3$ $Cd^{2+} = 0.7$ $Zn^{2+} = 12$	[45]
Zn^{2+} , Cd^{2+} , Pb^{2+}	In situ plated NCBFE	DPASV	180	$Zn^{2+} = 0.30$ $Cd^{2+} = 0.17$ $Pb^{2+} = 0.17$	[46]
Cd^{2+} , Pb^{2+}	MFSPCE	SWASV	120	$Cd^{2+} = 2.0$ $Pb^{2+} = 1.0$	[47]
Pb^{2+} , Cd^{2+} , Zn^{2+}	NC (Bpy)BiFE	SWASV	120	$Pb^{2+} = 0.08$ $Cd^{2+} = 0.12$ $Zn^{2+} = 0.56$	[21]
Zn^{2+} , Cd^{2+} , Pb^{2+}	Chemically synthesized Bi nanoparticles	SWASV	120	$Zn^{2+} = 0.52$ $Cd^{2+} = 0.45$ $Pb^{2+} = 0.41$	[48]
Zn^{2+} , Pb^{2+} , Cd^{2+}	Ex situ deposited bismuth	DPASV	60	$Zn^{2+} = 3.5$ $Pb^{2+} = 0.5$ $Cd^{2+} = 3.9$	[49]
Zn^{2+} , Pb^{2+} , Cd^{2+}	Nafion-G-HgFE	SWASV	120	$Zn^{2+} = 0.07$ $Cd^{2+} = 0.08$ $Pb^{2+} = 0.04$	[23]
Zn^{2+} , Pb^{2+} , Cd^{2+}	Gr-GC-HgFE	SWASV (individual analysis)	120	$Zn^{2+} = 0.04$ $Cd^{2+} = 0.11$ $Pb^{2+} = 0.14$	In this work
Zn^{2+} , Pb^{2+} , Cd^{2+}	Gr-GC-HgFE	SWASV (simultaneous analysis)	120	$Zn^{2+} = 0.08$ $Cd^{2+} = 0.05$ $Pb^{2+} = 0.14$	In this work

The slightly higher detection limits for simultaneous determinations can be attributed to the competition of the different metal ion species for active sites on the electrode surface in addition higher detection limits can also be attributed to the possible formation of intermetallic compounds between metals when present in the same solution [42]. Furthermore, the detection limits obtained with the Gr-GC-HgFE compares favourably with previously reported modified electrodes listed in Table 3 and, is thus suitable for trace analysis of Zn^{2+} , Cd^{2+} and Pb^{2+} .

3.12. Application of graphene – metal film electrodes

The Gr-GC-HgFE was applied to the analysis of Zn^{2+} , Cd^{2+} and Pb^{2+} in tap water samples, which was collected in our laboratory. To 19 ml of tap water was added 1 ml of 2 M acetate buffer (pH 4.6) to give a 0.1 M acetate buffered tap water sample. The electrode was established in the buffered tap water sample after adding the Hg^{2+} metal ions for *in situ* metal film preparation. SWASV analyses were performed by *in situ* deposition of the metal film and target metals, using a deposition time of 240 s. A longer deposition time was used in order to obtain a signal since a deposition time of 120 s was not adequate for real samples [50]. The amount of metal ions present in the tap water sample was determined by the standard additions method and are below the detection requirement set out by the Environmental Protective Agency (EPA) namely, Pb^{2+} ($15 \mu g L^{-1}$), Cd^{2+} ($5 \mu g L^{-1}$) and Zn^{2+} ($5 mg L^{-1}$); the results are given in Tables 4 and 5.

Table 4. Recoveries for the simultaneous determination of Zn^{2+} , Cd^{2+} and Pb^{2+} at the Gr-GC-HgFE.

Sample	Simultaneous analysis	Original ($\mu g L^{-1}$)	Added ($\mu g L^{-1}$)	Found ($\mu g L^{-1}$)	Recovery (%)
Tap water	Zn^{2+}	1.84 ± 0.05	3	4.58 ± 0.20	91
	Cd^{2+}	0.014 ± 0.0025	3	2.71 ± 0.08	90
	Pb^{2+}	0.45 ± 0.09	3	3.29 ± 0.16	95

*n = 3, where n is the number of replications

Table 5. Recoveries for the individual determination of Zn^{2+} , Cd^{2+} and Pb^{2+} at the Gr-GC-HgFE.

Sample	Individual analysis	Original ($\mu g L^{-1}$)	Added ($\mu g L^{-1}$)	Found ($\mu g L^{-1}$)	Recovery (%)
Tap water	Zn^{2+}	0.93 ± 0.020	3	3.9 ± 0.005	99
	Cd^{2+}	0.013 ± 0.002	3	2.5 ± 0.02	83
	Pb^{2+}	0.3 ± 0.090	3	3.3 ± 0.04	100

*n = 3, where n is the number of replications

In order to evaluate the accuracy of the method, tap water samples were spiked with known amounts of the target metal ions and then re-determined by using the method of standards additions. Tables 4 and 5 show that tap water samples spiked with $3 \mu\text{g L}^{-1}$ of the target metal ions gave good recoveries with the Gr-GC-HgFE namely, within 10% of the spiked amount. Much better recoveries were obtained for the individual analysis in comparison with simultaneous analysis except for, the recovery of Cd^{2+} which was better for the simultaneous analysis namely, 90 % compared to the 83% of the individual analysis. The slight increase in the recovery of Cd^{2+} during simultaneous determination of Cd^{2+} in a solution containing Zn^{2+} , Cd^{2+} and Pb^{2+} ions, is due to the improved diffusion coefficients of Cd^{2+} ions in a more conducting solution (i.e. the solution containing Zn^{2+} , Cd^{2+} and Pb^{2+} ions). The peak square wave anodic stripping peak current is directly proportional to the diffusion coefficient of the electroactive species.

5. CONCLUSIONS

A sensitive electrochemical sensor for determining Zn^{2+} , Cd^{2+} and Pb^{2+} was prepared based on the modification of a glassy carbon electrode with binding agent free graphene and in combination with an *in situ* deposited Hg-film (Gr-GC-HgFE). The sensor showed that by tuning the amount of graphene drop coated onto the glassy carbon surface together with an *in situ* deposited Hg-film resulted in larger currents and well- resolved stripping voltammetric peaks. Furthermore, the excellent stripping performance of the modified electrode showed it is capable of determining metal ions in tap water samples at sub-part per billion levels.

References

1. E. Merian, *Metals and their compounds in the environment: occurrence, analysis and biological relevance*. VCH Publishers, Weinheim, (1991) 1438.
2. L. Ebdon, L. Pitts, R. Cornelis, H. Crews, O.F.X. Donard, P. Quevauviller, (Eds). *Trace element speciation for environment, food and health; Royal Society of Chemistry: Cambridge*, (2001) 392.
3. G. H. Fernandez-Leborans, O. Yolanda, *Ecotoxicology Environmental Safety* 47 (2000) 266-276.
4. A. Sayari, S. Hamoudi, Y. Yang, *Chem. Mater.* 17 (2005) 212-216.
5. Heavy metals. <http://www.psr.org/environment-and-health/conforming toxics/heavymetals>. 25:02:2013.
6. J. Wang, *Stripping Analysis: Principles, Instrumentation, and Application*. VCH Publishers, Inc.: Deerfield Beach, Florida, (1985).
7. R.T. Kachoosangi, C. Banks X. Ji R. Compton, *Anal Sci.* 23 (2007) 283-289.
8. G. Sanna, M. Pilo, P.C. Piu, A. Tapparo, R. Seeber, *Anal. Chim. Acta* 415 (2000) 165-173.
9. M.J. Pinchin, J. Newham, *Anal. Chim. Acta* 90 (1977) 91-102.
10. F.N. Ertas, H.I. Gokcel, H. Tural, *Turk. J. Chem.* 24 (2000) 261- 267.
11. F. Miao, S. Wijeratne, U. Coskun, Y. Zhang, C.N. Lau, *Phase Coherent Transport of Charges in Graphene Quantum Billiard*. <http://arxiv.org/ftp/condmat/papers/0703/0703052.pdf> 26:02:2013.
12. W. Xinran, M.T. Scott, D. Hongjie, *J. Am. Chem. Soc.* 130 (2008) 8152-8153.
13. Y. Huafeng, L. Fenghua, S. Changsheng, H. Dongxue, Z. Qixian, L. Niu, I. Ari, *Mater. Chem.* 19 (2009) 4632-4638.
14. K.S. Novoselov, A.K. Geim, S.V. Morozov, D. Jiang, M.I. Katsnelson, I.V. Grigorieva, S.V. Dubonos, A.A. Firsov, *Nature* 438 (2005), 197-200.

15. N. Tombros, C. Jozsa, M. Popinciuc, H. Jonkman, W.B. Van, *Nature* 448 (2007) 571–574.
16. J. Fang.L. Ya-Li, F. Jian-Min, S. Dong.W. Yang-Yang, Y. Feng, F. Hou, *Mater. Chem.* 19 (2009) 9063–9067.
17. A.A. Balandin, S. Ghosh, W. Bao, I. Calizo, D. Teweldebrhan, F. Miao, C.N. Lau, . *Nano Lett.*, 8 (2008) 902–907.
18. D.A. Dikin, S. Stankovich, E.J. Zimney R.D. Piner, G.H.B. Dommett, G. Evmenenko, S.T. Nguyen, R.S. Ruoff, *Nature* 448 (2007), , 457–460.
19. S. Stankovich, D.A. Dikin, G.H.B. Dommett, K.M. Kohlhaas E.J. Zimney E.A. Stach R.D. Piner, S.T. Nguyen, R.S. Ruoff, *Nature* 442 (2006) 282–286.
20. J. Li, S. Guo, Y. Zhai, E. Wang, *Anal. Chim. Acta* 649 (2009)196–201.
21. J. Li, S. Guo, Y. Zhai, E. Wang, *Electrochem. Commun.* 11 (2009)1085–1088.
22. P.A. Khomyakov, G. Giovannetti, P.C. Rusu, G. Brocks, J. Van Den Brink, P.J. Kelly, *Phys. Rev* 79 (2009)195425-195437.
23. C.M. Willemse, K. Thhomelang, N. Jahed, P.G. Baker, E.I. Iwuoha, *Sensors* 11 (2011)3970-3987.
24. C.H.A. Wong, M. Pumera, *RSC Adv* 2 (2012)6068-6072.
25. W.S. Hummers R.E. Offeman *J. Am. Chem. Soc.* 80 (1958)1339-1339.
26. J. Shen, Y. Hu, M. Shi, X. Lu, C. Qin, C. Li, M. Ye, *Chem. Mater.* 21 (2009)3514–3520.
27. J. Shen, B. Yan, T. Li, Y. Long, N. Li, M. Ye, *Soft Matt.* 8 (2012)1831-1836.
28. S. Stankovich, D.A. Dikin, R.D. Piner, K.A. Kohlhaas, A. Kleinhammes, Y. Jia, Y. Wu, S.T. Nguyen, R.S. Ruoff, *Carbon* 45 (2007)1558–1565.
29. D. Zhang, X. Zhang, Y. Chen, C. Wang, Y. Ma, *Electrochim.Acta* 69 (2012)364-370.
30. D.C. Marcano, D.V. Kosynkin, J.M. Berlin, A. Sinitskii, Z. Sun, A. Slesarev, L.B. Alemany, W. Lu, J.M. Tour, *ACS NANO* 4 (2010)4806–4814.
31. Z. Li, W. Zhang, Y. Luo, J. Yang, J.G. Hou *J. Am. Chem. Soc.* 131 (2009) 6320–6321.
32. X. Zhou, T. Shi, H. Zhou, *Appl.surface sci.* 258 (2012), 6204 6211.
33. M.Z. Kassae, E. Motamedi, M. Majdi, *Chem. Engineering J.* 172 (2011)540-549.
34. J. Wu, Q. Tang, H. Sun, J. Lin, H. Ao, M. Huang, Y. Huang, *Langmuir* 24 (2008)4800-4805.
35. T.A. Pham, N.A. Kumar, Y.T. Jeong, *Synthetic Metals* 160 (2010)2028-2036.
36. Y. Zhu, M.D. Stoller, W. Cai, A. Velamakanni, R.D. Piner, D. Chen, R.S. Ruoff *J. Chem. Soc.* 132 (2010) 1227-1233.
37. Y. Zhu, S. Murali, W. Cai, X. Li, J.W. Suk, J.R. Potts, R.S. Ruoff, *Graphene and Graphene Oxide: Synthesis, Properties, and Applications*. *Advanced Materials* 2010, 22, 3906–3924. Journal or book
38. V. Singh, D. Joung, L. Zhai, S. Das, S.I. Khondaker, S. Seal, *Graphene based materials: Past, present and future*. *Science* 2011, 56, 1178–1271.
39. J. Shen, Y. Hu, M. Shi, X. Lu, C. Qin, C. Li, M. Ye, *Chem. Mater* 21 (2009)3514–3520.
40. N.A.F. Silva, R.A.E. Leitoa, M.J. Matos, . *Portugaliae Electrochim. Acta* 24 (2006)283-293.
41. W.J. Yi, Y. Li, G. Ran, H.Q. Luo, N.B. Li, *Microchim. Acta* 179 (2012)171-177.
42. K.C. Armstrong, C.E. Tatum, R.N. Dansby-Sparks, J.Q. Chambers, Z. Xue, *Talanta* 82 (2010) 675–680.
43. A.A. Ensafi, Z. Nazari, I. Fritsch, *Electroanalysis* 22 (2010)2551 – 2557.
44. G.G.A. Raquel, F. Clàudia, A. Enriqueta, M. Arben, *Analytica Chim. Acta* 627 (2008), 219–224.
45. G.H. Hwang, W.K. Han, J.S. Park, S.G. Kang,. *Talanta* 76 (2008)301-308.
46. H. Xu, L. Zeng, D. Huang, Y. Xian, L. Jin, *Food Chemistry* 109 (2008) 834-839.
47. M.F.M. Noh, I.E. Tothill, *Sains Malaysiana* 40 (2011)1153–1163.
48. M.A. Rico, M. Olivares-Marin, E.P. Gil, *Talanta* 80 (2009) 631–635.
49. N. Serrano, J.M. Diaz-Cruz, C. Ariño, M. Esteban, *Anal Bioanal Chem.* 396 (2010)1365–1369.
50. E.A. Sosnin, V.M. Batalova, E.Y. Buyanova, V.F. Tarasenko, *Proceedings Phys.Control* 1 (2003)349-351.